A frequency-domain approach to the analysis of stability and bifurcations in nonlinear systems described by differential-algebraic equations

A frequency-domain approach to the analysis of stability and bifurcations in nonlinear systems described by differential-algebraic equations

F. L. Traversa, F. Bonani and S. Donati Guerrieri

Politecnico di Torino, Dipartimento di Elettronica, Corso Duca degli Abruzzi 24, I-10129 Torino, Italy

SUMMARY

A general numerical technique is proposed for the assessment of the stability of periodic solutions and the determination of bifurcations for limit cycles in autonomous nonlinear systems represented by ordinary differential equations in the differential-algebraic form. The method is based on the harmonic balance (HB) technique, and exploits the same Jacobian matrix of the nonlinear system used in the Newton iterative numerical solution of the HB equations for the determination of the periodic steady state. To demonstrate the approach, it is applied to the determination of the bifurcation curves in the parameters' space of Chua's circuit with cubic nonlinearity, and to the study of the dynamics of the limit cycle of a Colpitts oscillator.

KEY WORDS: nonlinear systems; harmonic balance; stability; bifurcation

1. INTRODUCTION

The assessment of stability of periodic solutions of circuits and systems is of increasing interest, both from the standpoint of the determination of complex dynamical behaviours, such as bifurcations and routes to chaotic attractors, and of the definition of system stable operation [1]. From a circuit perspective, such an interest is directed both to autonomous (i.e. oscillators) and forced systems where the forcing term is a periodic function of time: in both cases, a periodic solution is assumed to exist. In order to study its stability, a perturbative approach is often employed [2], leading to Floquet theory which, ultimately, allows to assess the stability properties by estimating

a set of characteristic exponents called Floquet multipliers (FMs) (see Section 2). Furthermore, Floquet analysis plays a significant role in the analysis of phase noise in oscillators (see e.g. [3]). In this work, we shall focus on the case of autonomous systems admitting self-sustained oscillations: the extension to the study of the stability of periodic solutions of forced systems is straightforward.

The harmonic balance (HB) technique [4] is, in particular in the area of microwave and wireless circuit analysis and design, very common for the determination of periodic solutions due to its numerical efficiency, customarily related to the fact that the steady-state solution is directly determined, thus avoiding the computation of the transient part. On the other hand, in most cases time-domain approaches are exploited for studying the stability of the solution [5]. Only recently frequency-domain techniques have been proposed for the study of dynamic behaviour and bifurcations of nonlinear systems, often by making use of the describing function technique (i.e. HB with one harmonic only): see [6] and references therein. A more general, semi-analytical approach, able to include an HB description with an arbitrary number of harmonics, was proposed in [7], though limited to nonlinear systems that can be expressed in the Lur'e form. Finally, Mees [8] presented a general technique for the determination with HB of the Floquet Exponents of limit cycles of autonomous ordinary differential equations (ODEs) in canonical form.

In this paper we propose a general, fully numerical method for the direct estimation of the Floquet exponents (FEs) of a periodic solution based on the same Jacobian of the HB system already exploited in most numerical implementations of HB for the determination of the steady-state solution. Moreover, we propose an extended formulation valid not only for dynamical systems represented by ODEs in the canonical form, but also applicable to differential-algebraic equations (DAEs). This makes the methodology directly implementable even into commercial circuit-oriented simulation CAD tools, at least if the circuit considered is lumped and if the system Jacobian is made available.[§] The proposed technique is applied to the simulation of two dynamical systems: Chua's circuit, which exhibits a very complex dynamic behaviour with a large number of bifurcations, and a classical Colpitts oscillator.

The paper is structured as follows: a brief review of the Floquet theory for systems described by DAEs is the subject of Section 2, while the frequency-domain approach to the determination of the corresponding FEs and multipliers is presented in Section 3: the generalized eigenvalue problem (27) is shown to allow the numerical computation of the FEs. Two examples of application are discussed in Section 4, and finally Section 5 is devoted to the conclusions.

2. FLOQUET THEORY FOR DAEs

DAEs are very common in the analysis of nonlinear electrical circuits, since the popular modified node analysis (MNA) [9] results in a mathematical description of the Kirchhoff laws and of the circuit elements' constitutive relationships in the form of a system of DAEs. In abstract form, we are interested in a vector autonomous differential system written as

$$\frac{\mathrm{d}}{\mathrm{d}t}\mathbf{q}(\mathbf{x}) + \mathbf{g}(\mathbf{x}) = \mathbf{0} \tag{1}$$

[§] In most cases, the system Jacobian is not available to the user; therefore, the implementation of this approach should be carried out by the software vendor.

where $\mathbf{x}(t) \in \mathbb{R}^M$ is an M-dimensional real continuous vector function of time, and $\mathbf{q}, \mathbf{g} : \mathbb{R}^M \to \mathbb{R}^M$ are continuous nonlinear functions. For the sake of our discussion, we assume that a nontrivial T-periodic solution $\mathbf{x}_s(t)$ (i.e. $T>0$ and $\mathbf{x}_s(t+T)=\mathbf{x}_s(t)\ \forall t \in \mathbb{R}$) exists, called a limit cycle for Equation (1).

The aim of Floquet theory is to develop a perturbative analysis of Equation (1) around the limit cycle $\mathbf{x}_s(t)$, thus allowing for an assessment of the (local) stability properties of the limit cycle itself. Floquet theory was originally developed for the solution of periodically time-varying systems of linear ODEs [2] such as

$$\dot{\mathbf{x}} = \mathbf{B}(t)\mathbf{x} \tag{2}$$

where $\mathbf{B}(t) : \mathbb{R} \to \mathbb{R}^{M\times M}$ is a continuous T-periodic matrix function of time and $\dot{\mathbf{x}}$ denotes the time derivative of $\mathbf{x}(t)$. Recently, it has been extended to the solution of linearized DAEs in [10, 11], at least in the case of index-1 equations. We shall now briefly review the main results, following the formulation developed in [11].

According to the discussion in [11], the assessment of the stability properties of the steady-state solution $\mathbf{x}_s(t)$ of Equation (1) requires to decompose the solution $\mathbf{x}(t)$ of the system forced by a small perturbation into a phase (α) and an orbital ($\mathbf{y}$) component: $\mathbf{x}(t)=\mathbf{x}_s[t+\alpha(t)]+\mathbf{y}(t)$. A detailed analysis allows us to demonstrate that stability is ultimately related to the solution of the homogeneous system obtained by linearizing (1) around $\mathbf{x}_s(t)$

$$\frac{\mathrm{d}}{\mathrm{d}t}[\mathbf{C}(t)\mathbf{z}(t)] - \mathbf{A}(t)\mathbf{z}(t) = \mathbf{0} \tag{3}$$

where the two matrix functions $\mathbf{C}$ and $\mathbf{A}$ are T-periodic, since they are the Jacobian of $\mathbf{q}$ and $\mathbf{g}$, respectively, evaluated in the limit cycle $\mathbf{x}_s(t)$:

$$\mathbf{C}(t) = \left.\frac{\mathrm{d}\mathbf{q}}{\mathrm{d}\mathbf{x}}\right|_{\mathbf{x}_s(t)}, \quad \mathbf{A}(t) = -\left.\frac{\mathrm{d}\mathbf{g}}{\mathrm{d}\mathbf{x}}\right|_{\mathbf{x}_s(t)} \tag{4}$$

Notice that $\mathbf{C}$ is not necessarily full rank: however, we assume that $\mathrm{rank}\{\mathbf{C}(t)\}=m\leqslant M$ does not depend on t [11].

According to [2, 11], the solution of Equation (3) can be expressed in terms of the *fundamental state-transition matrix* $\mathbf{\Phi}(t,s)$, meaning that solution $\mathbf{z}(t;\mathbf{z}_0)$ of Equation (3) satisfying the initial condition $\mathbf{z}(0;\mathbf{z}_0)=\mathbf{z}_0$[¶] is given by

$$\mathbf{z}(t;\mathbf{z}_0) = \mathbf{\Phi}(t,0)\mathbf{z}_0 \tag{5}$$

The fundamental state-transition matrix can be expressed as [2, 11]

$$\mathbf{\Phi}(t,s) = \mathbf{U}(t)\mathrm{e}^{(t-s)\mathbf{D}}\mathbf{V}(s)\mathbf{C}(s) \tag{6}$$

where $\mathbf{U}, \mathbf{D}, \mathbf{V} \in \mathbb{R}^{M\times M}$, and $\mathbf{U}(t)$, $\mathbf{V}(t)$ are T-periodic invertible matrix functions such that

$$\mathbf{V}(t)\mathbf{C}(t)\mathbf{U}(t) = \begin{bmatrix} \mathbf{I}_m & \mathbf{0} \\ \mathbf{0} & \mathbf{0} \end{bmatrix} \tag{7}$$

[¶]We assume here that $\mathbf{z}_0 \in S(0)$, where $S(t)$ is the m-dimensional subspace where the index-1 equation (3) has solutions [11].

$\mathbf{I}_m$ being the identity matrix of size m. Furthermore

$$\exp(t\mathbf{D}) = \mathrm{diag}\{\exp(\mu_1 t), \ldots, \exp(\mu_m t), 0, \ldots, 0\} \tag{8}$$

is a diagonal matrix: the m coefficients of μ_k are the FEs of system (3), while $\lambda_k = \exp(\mu_k T)$ are the corresponding FMs. Notice that Equation (8) implies that $\mathbf{D}$ has $M - m$ eigenvalues equal to $-\infty$, i.e. system (3) has $M - m$ FMs equal to 0. By denoting as $\mathbf{u}_k(t)$ the columns of $\mathbf{U}(t)$, and as $\mathbf{v}_k^{\mathrm{T}}(t)$ the rows of $\mathbf{V}(t)$, the following remarks hold [11]:

1. for $1 \leqslant k \leqslant m$, $\mathbf{z}(t) = \mathbf{u}_k(t)\exp(\mu_k t)$ is a solution of Equation (3) with initial condition $\mathbf{z}(0) = \mathbf{u}_k(0)$;
2. for $1 \leqslant k \leqslant m$, $\tilde{\mathbf{z}}(t) = \mathbf{v}_k(t)\exp(-\mu_k t)$ is a solution of system

$$\mathbf{C}^{\mathrm{T}}(t)\frac{\mathrm{d}}{\mathrm{d}t}\tilde{\mathbf{z}}(t) + \mathbf{A}^{\mathrm{T}}(t)\tilde{\mathbf{z}}(t) = \mathbf{0} \tag{9}$$

   with initial condition $\tilde{\mathbf{z}}(0) = \mathbf{v}_k(0)$; Equation (9) represents the *adjoint system* associated with Equation (3).

Since $\mathbf{u}_k(t)$ is associated with the corresponding FE μ_k, it is denoted as the *Floquet eigenvector* associated with μ_k.

Substituting $\mathbf{z}(t) = \mathbf{u}_k(t)\exp(\mu_k t)$ into Equation (3), the FE and Floquet eigenvectors are shown to satisfy

$$\mu_k \mathbf{C}(t)\mathbf{u}_k(t) + \mathbf{C}(t)\dot{\mathbf{u}}_k(t) = [\mathbf{A}(t) - \dot{\mathbf{C}}(t)]\mathbf{u}_k(t) \tag{10}$$

2.1. Stability and bifurcations in autonomous DAEs

According to the discussion in [11], for an autonomous system $\dot{\mathbf{x}}_{\mathrm{s}}(t) = \mathrm{d}\mathbf{x}_{\mathrm{s}}/\mathrm{d}t$ is a solution of the linearized system (3): this means that $\lambda_1 = 1$ is one of the FMs associated with the limit cycle itself, with the corresponding Floquet eigenvector $\mathbf{u}_1(t) = \dot{\mathbf{x}}_{\mathrm{s}}(t)$. Furthermore, the state-transition matrix (6) can be decomposed according to [11]:

$$\mathbf{\Phi}(t, s) = \sum_{k=1}^{m} \mathrm{e}^{\mu_k (t-s)}\mathbf{u}_k(t)\mathbf{v}_k^{\mathrm{T}}(s)\mathbf{C}(s) \tag{11}$$

As a consequence, for the limit cycle of the autonomous system to be *asymptotically stable*, all the remaining $m - 1$ FMs must lie within the unit circle in the complex plane, i.e. $|\lambda_k| < 1$ $\forall k = 2, \ldots, m$.

Concerning bifurcations, the conditions for a fold and a flip (period doubling) phenomenon to take place are simply that one FM equals 1 or -1, respectively [2, 7].

3. FREQUENCY-DOMAIN DETERMINATION OF FLOQUET MULTIPLIERS

The aim of this section is to introduce a novel technique, amenable to be implemented in circuit analysis CAD tools, for the evaluation of the FMs associated with a limit cycle completely in the frequency domain. The main reason behind the development of such an approach is that the HB technique is probably the most popular and effective tool for evaluating the limit cycle in

microwave and RF nonlinear circuits, both in the case of forced and autonomous systems.[‖] In order to introduce the algorithm, we shall make use of the formalism presented in [4, 7].

3.1. HB formulation

Let us consider a T-periodic scalar real continuous and differentiable function $x(t)$, represented in the frequency domain by a truncated Fourier series, made of N_{H} harmonics plus the DC component

$$x(t) = \sum_{h=0}^{N_{\mathrm{H}}} x_h(t), \quad x_h(t) = \begin{cases} x_{\mathrm{c0}}^{\mathrm{f}}, & h = 0 \\ x_{\mathrm{ch}}^{\mathrm{f}} \cos(h\omega t) + x_{\mathrm{sh}}^{\mathrm{f}} \sin(h\omega t), & h = 1, \ldots, N_{\mathrm{H}} \end{cases} \tag{12}$$

where $x_{\mathrm{ch}}^{\mathrm{f}}$ and $x_{\mathrm{sh}}^{\mathrm{f}}$ are the (cosine and sine) harmonic amplitudes associated with the hth harmonic of (angular) frequency $h\omega$ ($\omega = 2\pi/T$). Of course, the finite sum in Equation (12) is just an approximation of the full Fourier representation, necessary for computational purposes: we shall assume that N_{H} is large enough to approximate the 'real' $x(t)$ within an acceptable error. By collecting the harmonic amplitudes into a column vector

$$\mathbf{x}^{\mathrm{f}} = [x_{\mathrm{c0}}^{\mathrm{f}}, x_{\mathrm{c1}}^{\mathrm{f}}, x_{\mathrm{s1}}^{\mathrm{f}}, \ldots, x_{\mathrm{c}N_{\mathrm{H}}}^{\mathrm{f}}, x_{\mathrm{s}N_{\mathrm{H}}}^{\mathrm{f}}]^{\mathrm{T}} \tag{13}$$

and defining the $2N_{\mathrm{H}} + 1$ time samples $t_h = hT/(2N_{\mathrm{H}} + 1)$ ($h = 1, \ldots, 2N_{\mathrm{H}} + 1$) equally spaced into the period $]0, T]$, an invertible linear operator $\mathbf{\Gamma}$ allows for the time–frequency transformation [4, 7]

$$\mathbf{x}^{\mathrm{f}} = \mathbf{\Gamma}\mathbf{x} \iff \mathbf{x} = \mathbf{\Gamma}^{-1}\mathbf{x}^{\mathrm{f}} \tag{14}$$

where we have denoted by $\mathbf{x}$ the column vector collecting the time samples of $x(t)$:

$$\mathbf{x} = [x(t_1), x(t_2), \ldots, x(t_{2N_{\mathrm{H}}+1})]^{\mathrm{T}} \tag{15}$$

The expression for the transformation from harmonic components to time samples can be easily derived from Equation (12)

$$\mathbf{\Gamma}^{-1} = \begin{bmatrix} 1 & \gamma_{1,1}^{\mathrm{c}} & \gamma_{1,1}^{\mathrm{s}} & \cdots & \gamma_{1,N_{\mathrm{H}}}^{\mathrm{c}} & \gamma_{1,N_{\mathrm{H}}}^{\mathrm{s}} \\ 1 & \gamma_{2,1}^{\mathrm{c}} & \gamma_{2,1}^{\mathrm{s}} & \cdots & \gamma_{2,N_{\mathrm{H}}}^{\mathrm{c}} & \gamma_{2,N_{\mathrm{H}}}^{\mathrm{s}} \\ \vdots & \vdots & \vdots & & \vdots & \vdots \\ 1 & \gamma_{2N_{\mathrm{H}}+1,1}^{\mathrm{c}} & \gamma_{2N_{\mathrm{H}}+1,1}^{\mathrm{s}} & \cdots & \gamma_{2N_{\mathrm{H}}+1,N_{\mathrm{H}}}^{\mathrm{c}} & \gamma_{2N_{\mathrm{H}}+1,N_{\mathrm{H}}}^{\mathrm{s}} \end{bmatrix} \tag{16}$$

where γ^{c} and γ^{s} are given by

$$\gamma_{p,q}^{\mathrm{c}} = \cos(q\omega t_p) = \cos\left(\frac{q2\pi p}{2N_{\mathrm{H}} + 1}\right), \quad \gamma_{p,q}^{\mathrm{s}} = \sin(q\omega t_p) = \sin\left(\frac{q2\pi p}{2N_{\mathrm{H}} + 1}\right) \tag{17}$$

Notice that operator $\mathbf{\Gamma}$, due to the choice of the time samples, is independent of ω, and therefore, the formulation can be exploited for the determination of the limit cycle of autonomous systems [4, 7].

[‖] In the latter case, the frequency $\omega = 2\pi/T$ of the limit cycle is also an unknown to be solved for, see e.g. [4].

Also the time derivative of $x(t)$ can be expressed in the frequency domain as a function of the harmonic components $\mathbf{x}^{\mathrm{f}}$. An explicit evaluation of $\dot{x}(t)$ from Equation (12) leads to [7]:

$$\dot{\mathbf{x}}^{\mathrm{f}} = \boldsymbol{\Gamma}\dot{\mathbf{x}} = \omega\boldsymbol{\Omega}\mathbf{x}^{\mathrm{f}} \tag{18}$$

where $\dot{\mathbf{x}}$ denotes the collection of time samples of $\dot{x}(t)$, $\dot{\mathbf{x}}^{\mathrm{f}}$ are the harmonic components of $\dot{x}(t)$, and $\boldsymbol{\Omega}$ is a constant $(2N_{\mathrm{H}}+1)\times(2N_{\mathrm{H}}+1)$ matrix given by

$$\boldsymbol{\Omega} = \begin{bmatrix} 0 & 0 & 0 & 0 & 0 & \dots & 0 & 0 \\ 0 & 0 & 1 & 0 & 0 & \dots & 0 & 0 \\ 0 & -1 & 0 & 0 & 0 & \dots & 0 & 0 \\ 0 & 0 & 0 & 0 & 2 & \dots & 0 & 0 \\ 0 & 0 & 0 & -2 & 0 & \dots & 0 & 0 \\ \vdots & \vdots & \vdots & \vdots & \vdots & & \vdots & \vdots \\ 0 & 0 & 0 & 0 & 0 & \dots & 0 & N_{\mathrm{H}} \\ 0 & 0 & 0 & 0 & 0 & \dots & -N_{\mathrm{H}} & 0 \end{bmatrix} \tag{19}$$

Equations (14)–(19) can be exploited for the definition of the HB system used for the determination of the limit cycle harmonic amplitudes $\mathbf{x}_{\mathrm{s}}^{\mathrm{f}}$, both for the cases of forced and autonomous systems (see [4] for details), in the latter case by taking into account that the inclusion of the additional unknown ω (the limit cycle angular frequency) can be treated by arbitrarily fixing one of the harmonic amplitudes (i.e. fix the phase reference of the limit cycle) [4, 7]. For instance, a possible choice is to set to zero the sine amplitude of the first harmonic of the first component of $\mathbf{x}_{\mathrm{s}}(t)$, i.e. $x_{\mathrm{s},1,\mathrm{s}1}^{\mathrm{f}} = 0$.

3.2. HB-based algorithm for FM determination

The frequency-domain evaluation of the FMs is based on a HB formulation of Equation (10). To keep the notation as simple as possible, we shall denote by $\mathbf{u}_k$ the vector of collected time samples for the vector function of time $\mathbf{u}_k(t)$, ordered according to its components $u_{p,k}(t)$ $(p = 1, \dots, M)$:

$$\mathbf{u}_k = [u_{k,1}(t_1), \dots, u_{k,1}(t_{2N_{\mathrm{H}}+1}), \dots, u_{k,M}(t_1), \dots, u_{k,M}(t_{2N_{\mathrm{H}}+1})]^{\mathrm{T}} \tag{20}$$

$\mathbf{u}_k^{\mathrm{f}}$ is the corresponding collection of harmonic components

$$\mathbf{u}_k^{\mathrm{f}} = [u_{k,1,\mathrm{c}0}^{\mathrm{f}}, u_{k,1,\mathrm{c}1}^{\mathrm{f}}, u_{k,1,\mathrm{s}1}^{\mathrm{f}}, \dots, u_{k,1,\mathrm{s}N_{\mathrm{H}}}^{\mathrm{f}}, \dots, u_{k,M,\mathrm{c}0}^{\mathrm{f}}, \dots, u_{k,M,\mathrm{s}N_{\mathrm{H}}}^{\mathrm{f}}]^{\mathrm{T}} \tag{21}$$

so that the relationship between the time samples and the frequency components for the vector functions is a simple generalization of the scalar one (14)

$$\mathbf{u}_k^{\mathrm{f}} = \boldsymbol{\Gamma}_M \mathbf{u}_k \iff \mathbf{u}_k = \boldsymbol{\Gamma}_M^{-1}\mathbf{u}_k^{\mathrm{f}} \tag{22}$$

where $\boldsymbol{\Gamma}_M$ is a block-diagonal linear operator made of M blocks each equal to $\boldsymbol{\Gamma}$:

$$\boldsymbol{\Gamma}_M = \mathrm{diag}\{\boldsymbol{\Gamma}, \dots, \boldsymbol{\Gamma}\} \quad M \text{ blocks} \tag{23}$$

A direct application of Equation (18) leads also to

$$\dot{\mathbf{u}}_k^{\mathrm{f}} = \boldsymbol{\Gamma}_M \dot{\mathbf{u}}_k = \omega \boldsymbol{\Omega}_M \mathbf{u}_k^{\mathrm{f}} \tag{24}$$

where $\boldsymbol{\Omega}_M$ is a block-diagonal linear operator made of M blocks each equal to $\boldsymbol{\Omega}$:

$$\boldsymbol{\Omega}_M = \mathrm{diag}\{\boldsymbol{\Omega}, \ldots, \boldsymbol{\Omega}\} \quad M \text{ blocks} \tag{25}$$

Similar arguments can be applied to show that for the matrix T-periodic function $\dot{\mathbf{C}}(t)$ the following relationship holds**:

$$\boldsymbol{\Gamma}_M[\dot{\mathbf{C}}\mathbf{u}_k + \mathbf{C}\dot{\mathbf{u}}_k] = \omega \boldsymbol{\Omega}_M \boldsymbol{\Gamma}_M(\mathbf{C}\mathbf{u}_k) = \omega \boldsymbol{\Omega}_M \hat{\mathbf{C}} \mathbf{u}_k^{\mathrm{f}} \tag{26}$$

where $\mathbf{C}$ and $\dot{\mathbf{C}}$ are $(2N_{\mathrm{H}}+1)M \times (2N_{\mathrm{H}}+1)M$ constant matrices built up by expanding each element of matrix functions $\mathbf{C}(t)$ and $\dot{\mathbf{C}}(t)$, respectively, with a diagonal block of the corresponding time samples, and $\hat{\mathbf{C}} = \boldsymbol{\Gamma}_M \mathbf{C} \boldsymbol{\Gamma}_M^{-1}$.

Multiplying by $\boldsymbol{\Gamma}_M$ the time samples of Equation (10) and making use of the identity $\boldsymbol{\Gamma}_M^{-1}\boldsymbol{\Gamma}_M = \mathbf{I}_{(2N_{\mathrm{H}}+1)M}$ and of Equations (22), (24), and (26), the following generalized eigenvalue problem is found

$$(\hat{\mathbf{A}} - \omega \boldsymbol{\Omega}_M \hat{\mathbf{C}}) \mathbf{u}_k^{\mathrm{f}} = \mu_k \hat{\mathbf{C}} \mathbf{u}_k^{\mathrm{f}} \tag{27}$$

for the FEs and the harmonic amplitudes of the associated Floquet eigenvectors, where:

$$\hat{\mathbf{A}} = \boldsymbol{\Gamma}_M \mathbf{A} \boldsymbol{\Gamma}_M^{-1} \tag{28}$$

From an implementation standpoint, it is worth noticing that matrices $\mathbf{C}$ and $\mathbf{A}$ are the Jacobian matrices of the nonlinear functions $\mathbf{q}$ and $-\mathbf{g}$ evaluated in the steady-state limit cycle. Since the HB system is generally solved by exploiting Newton iterations, such Jacobians are directly available for the FM estimation.

The size of the generalized eigenvalue problem (27) is $(2N_{\mathrm{H}}+1)M \times (2N_{\mathrm{H}}+1)M$, therefore, the number of FEs numerically derived from a full eigenvalue determination is $(2N_{\mathrm{H}}+1)M$. According to the remark in [2], the FEs are actually infinite in number: there are m independent FMs, which correspond to an infinite set of FEs distributed in the complex plane along m vertical lines. For each line k, the infinite FEs $\mu_{k,q}$ are located at a constant distance equal to $\mathrm{j}2\pi/T$ ($\mathrm{j} = \sqrt{-1}$) from each other:

$$\mu_{k,q} = \mu_{k,0} + q\mathrm{j}\frac{2\pi}{T}, \quad q \in \mathbb{Z} \Longrightarrow \lambda_k = \mathrm{e}^{\mu_{k,q}T} = \mathrm{e}^{\mu_{k,0}T + q\mathrm{j}2\pi} = \mathrm{e}^{\mu_{k,0}T} \tag{29}$$

The truncated relationship (27) yields an approximate estimation of the FEs $\mu_{k,q}$. In fact, as discussed in Section 4, the numerical distribution in the complex plane of FEs evaluated from Equation (27) tends to diverge from the theoretical one moving far from the eigenvalues nearest to the real axis. For this reason, numerical accuracy requires the inclusion of the FEs with minimal (absolute value of) imaginary part for the FM estimation. This remark, justified here only on the basis of numerical results, can be supported by a more rigorous derivation which is neglected here for the sake of conciseness and will be published elsewhere.

**Corrections made to Equations (26)–(28) and to the paragraph following Equation (26) after initial online publication.

Furthermore, in order to reduce the computational burden for very large systems, specialized numerical algorithms allowing for the calculation of the eigenvalues in Equation (27) in a predefined region of the complex plane [12] can also be exploited.

3.3. Frequency-domain estimation of bifurcation conditions

Let us consider that the dynamical system depends on a parameter α, used as a bifurcation parameter. The limit cycle's FEs are the solutions of the generalized eigenvalue problem (27), where all the terms apart from $\mathbf{\Omega}_M$ depend on the parameter α: in order to satisfy the bifurcation condition, we have to determine a value α_0 of the parameter (if it exists) which makes one of the limit cycle FMs of magnitude equal to 1 (see Section 2.1). The bifurcation parameter value α_0 satisfies the equation

$$\lambda_{k_0}(\alpha_0) = \begin{cases} +1 & \text{for a fold bifurcation} \\ \mathrm{e}^{\mathrm{j}\phi}, \quad \phi \in \mathbb{R}\backslash\{0, \pi\} & \text{for a Neimark–Sacker bifurcation} \\ -1 & \text{for a flip bifurcation} \end{cases} \tag{30}$$

where k_0 is the index labelling the FM taking the value required by the bifurcation condition. Notice that, as discussed in Section 2.1, for a fold bifurcation to occur in an autonomous system a second FM must be equal to $+1$, besides the FM equal to $+1$ always present in such a case.

In this work, Equation (30) is numerically solved by applying the standard secant method [13]. This corresponds to build up a sequence $\{\alpha_i\}$ of values of the parameter which, if the secant approach converges, tends to α_0: for each iteration of the numerical approach (i.e. for each parameter value α_i) the limit cycle is determined solving the HB problem, and the corresponding FMs are estimated solving Equation (27). Then, the FM closest to the required value is chosen (this amounts to select k_0) and is used for determining the new approximation of the solution.

4. EXAMPLES OF APPLICATION

The methodology described in Section 3 has been applied to the simulation of two autonomous systems: we have considered the well-known Chua's circuit, characterized by a very complex dynamic behaviour, and a standard Colpitts oscillator. In order to determine the limit cycles, we have implemented the homotopy scheme proposed in [14, 15] which enables us to compute the autonomous working point starting from a nonautonomous simulation, thus avoiding the use of several (often randomly chosen) initial conditions to find different limit cycles.

4.1. Chua's circuit

The first example of application is the well-known Chua's circuit with cubic nonlinearity [16], characterized by the normalized equations

$$\begin{aligned} \dot{x} &= \alpha[y - n(x) - x] \\ \dot{y} &= x - y + z \\ \dot{z} &= -\beta y \end{aligned} \tag{31}$$

where α, β are real parameters, and the nonlinear function $n(x)$ is a cubic polynomial:

$$n(x) = -\tfrac{8}{7}x + \tfrac{4}{63}x^3 \tag{32}$$

This system is in a canonical form (i.e. $\mathbf{q}$ in Equation (1) is the identity operator), and is characterized by $M = m = 3$. Thus,

$$\mathbf{C}(t) = \mathbf{I}_3 \Longrightarrow \hat{\mathbf{C}} = \mathbf{I}_3, \quad \hat{\mathbf{A}}' = \hat{\mathbf{A}} \tag{33}$$

Chua's circuit was chosen as a first case study because it allows for a direct comparison with the results in [7], where its bifurcations were studied in the frequency domain with a different approach for the estimation of the FMs.

As a function of the parameters α and β, Equation (31) gives rise to a wide variety of dynamic behaviours [7, 16]: for $\alpha<7$ two equilibria exist, symmetric with respect to the origin of the state space. As α is increased, first two asymmetric limit cycles are born from a Hopf bifurcation of the two equilibria [16], followed for an even larger α by two further symmetric limit cycles (one stable and one unstable). Figure 1 shows the relationship between the cycle period T and the system parameter α ($\beta = 15$ is held constant) for both the asymmetric and symmetric limit cycles. Simulations are carried out by solving the HB system with $15 \leqslant N_{\mathrm{H}} \leqslant 50$ (the actual value of N_{H} is chosen by controlling the relative error in the solution between simulations with N_{H} and $N_{\mathrm{H}} + 1$ harmonics) for the determination of the steady-state solution, and changing the initial conditions in order to detect the various limit cycles. Notice that for α close to 11.5377 (and $T \approx 11.514$) a second symmetric cycle appears, leading to the dash-dotted curve in the inset of Figure 1.

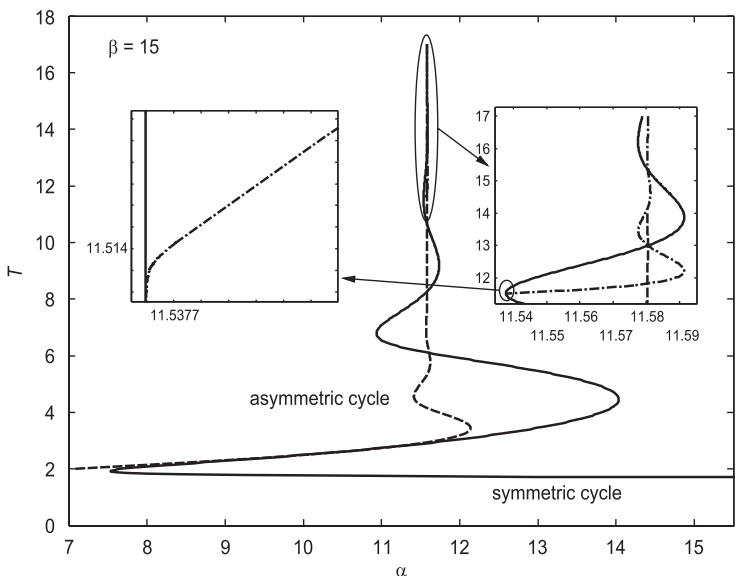

Figure 1. Chua's circuit: α-parameter dependence of the limit cycle period T for symmetric and asymmetric cycles. Symmetric cycle: continuous and dash-dotted lines. Asymmetric cycle: dashed line.

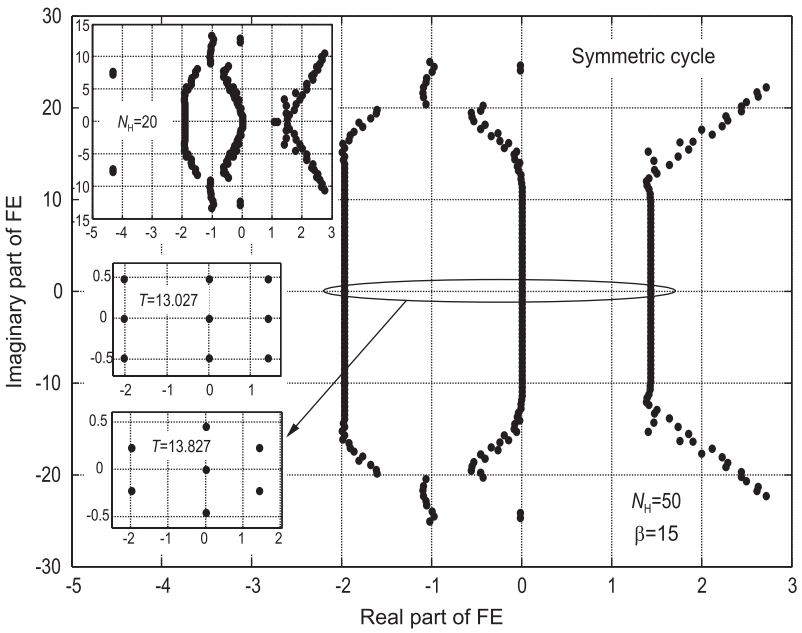

Figure 2. Chua's circuit: example of FE distribution in the complex plane for the symmetric limit cycle ($N_{\mathrm{H}} = 50$, $T = 13.827$). Top inset: FE distribution for $N_{\mathrm{H}} = 20$, $T = 13.827$. Middle inset: zoom of the FE distribution for $T = 13.027$. Bottom inset: zoom of the FE distribution for $T = 13.827$.

The stability of such limit cycles is studied according to the approach presented in Section 3.2, i.e. by evaluating their three FMs. As expected for an autonomous system, one of them is always equal to 1. The distribution in the complex plane of the FEs calculated from the generalized eigenvalue problem (27) is shown in Figure 2 for the case of the principal symmetric cycle (continuous line of Figure 1, $\beta = 15$ and $T = 13.827$). As discussed in Section 3.2, the numerically calculated FEs are distributed on vertical lines in the complex plane according to Equation (29). The position of the FEs tends to diverge from the theoretical one as the imaginary part becomes larger, thus suggesting that for a better numerical accuracy, the FMs must be calculated by choosing the FEs with minimal imaginary part: this heuristic remark is also supported by a more rigorous analysis, omitted here for the sake of brevity. The FEs are calculated including $N_{\mathrm{H}} = 50$ harmonics in the HB simulation: for comparison, the same system is solved for $N_{\mathrm{H}} = 20$ (see top inset in Figure 2), showing a much worse distribution of FEs in the complex plane. Notice that such a large number of harmonics is necessary for an accurate estimation of the FEs is related to the properties of this limit cycle, which is unstable with a very large FM: our numerical experiments show that for lower values of the FM magnitude a satisfactory accuracy is achieved with a much lower N_{H}. As a final remark, the bottom inset of Figure 2 shows that, besides the 0 FE, the other two FMs correspond to FEs with minimal imaginary part different from zero. They actually give rise to two FMs only, because their imaginary part is exactly equal to π/T. For comparison, the middle inset of Figure 2 shows the FEs with minimal imaginary part for a different symmetric limit cycle ($T = 13.027$), which are all real.

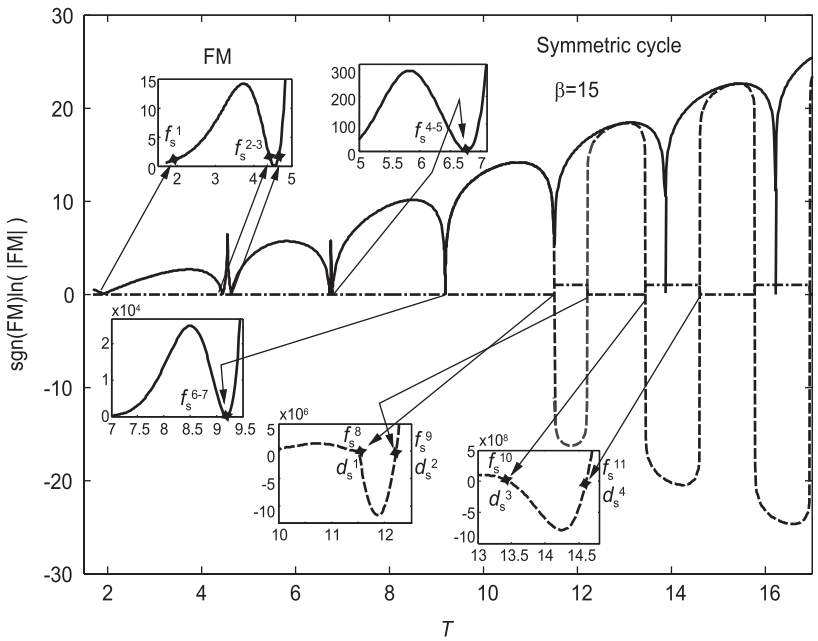

Figure 3. Chua's circuit: T dependence of the real part of the FM responsible for bifurcations of the symmetric limit cycles. The dash-dotted line represents a function equal to 0 if the FE nearest to the real axis is real, and to 1 if it is complex.

In order to assess the stability properties of the symmetric limit cycles, the real part of the FM responsible for bifurcations[††] (the principal FM defined in [7]) is shown in Figure 3 as a function of the cycle period T: the continuous curve corresponds to the symmetric cycle present for $\alpha = 2$, while the dashed line corresponds to the symmetric cycle detected for $\alpha > 11.5377$ only. In the first case, the FM is always nonnegative, and, therefore, it undergoes fold bifurcations only: they are denoted as f_s^k ($k \in \mathbb{N}$) [7], where the higher the value of k, the larger the corresponding cycle period. For the second symmetric cycle, on the other hand, the FM can become negative, thus giving rise also to period-doubling bifurcations here named as d_s^k ($k \in \mathbb{N}$): notice that these bifurcations, not discussed in [7], require the corresponding FE to be complex. As T is increased, the sequence of bifurcations $f_s^{k_1}$–$d_s^{k_2}$–$d_s^{k_2+1}$–$f_s^{k_1+1}$ is always observed: correspondingly, the FEs are real, complex, and real again (see the dash-dotted line in Figure 3). As a further insight, we consider in Figure 4 the evolution as a function of T of the two FEs not identically equal to 0 between f_s^2 and f_s^3: both are always real, and in f_s^2 and f_s^3 one of them is equal to 0, the other is negative. As T increases, the values of the two FEs get closer, eventually becoming equal for T slightly larger than 4.55. This corresponds to a collision between the corresponding FMs. Then, the two FEs diverge again, one increasing until f_s^3 is reached. This pattern is followed for all the transitions between two consecutive fold bifurcations.

[††]For the other two FMs, one is always equal to 1, the other is always stable.

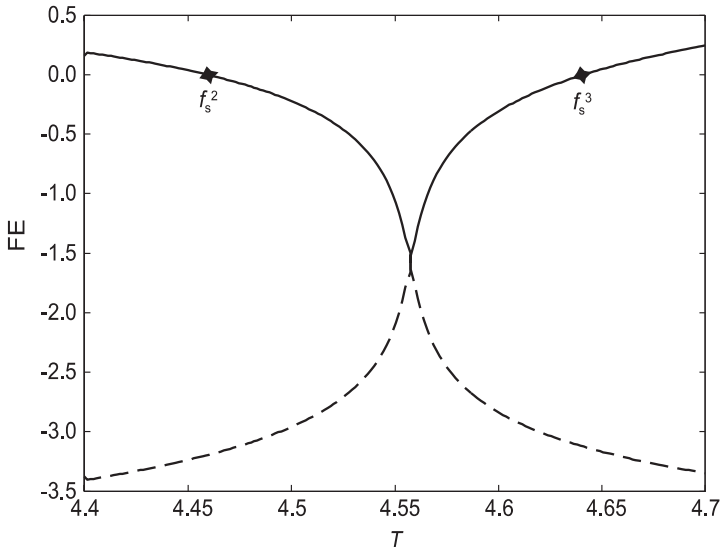

Figure 4. Chua's circuit: evolution of the FEs not identically equal to 0 for the symmetric limit cycle between f_s^2 and f_s^3 as a function of the cycle period T.

A similar analysis is carried out for the study of the bifurcations of the asymmetric limit cycle. Figure 5 reports the real part of the principal FM [7] as a function of the asymmetric cycle period T. The first flip bifurcation d_a gives rise to the spiral attractor [7], then the cycle becomes unstable until a sequence of period doubling (d_a^1) and fold (f_a^1) bifurcations is observed. Starting from d_a^1, as T grows bifurcations follow the sequence d_a^k–f_a^k–f_a^{k+1}–d_a^{k+1}, where the cycle is stable between d_a^k–f_a^k and f_a^{k+1}–d_a^{k+1} only. In particular, in the regions of stability between the flip and fold bifurcations the principal FM becomes complex, and thus the other FM not identically equal to 1 must be the complex conjugate of the former. This is demonstrated in Figure 6, where the two FMs not identically equal to 1 for the asymmetric cycle are shown as a function of T between d_a^3 and f_a^3: at d_a^3, the principal FM is equal to -1 and is represented in the figure by circles, while the other FM is real and close to 0 (see the stars in Figure 6). As T is increased, the principal FM increases and the other decreases, both remaining real: when the two FMs collide, both become complex with increasing real part, up to a T value for which they collide again becoming real. The role of the two FMs is now exchanged, since the circle's real part is now a decreasing function of T, while the stars exhibit a growing real part which takes them to the fold bifurcation f_a^3 (and, thus, this becomes the principal FM responsible for the bifurcation).

Finally, some bifurcation curves in the parameter space (α, β) have been computed according to the method described in Section 3.3 by means of continuation as a function of the β parameter, choosing as a starting point the bifurcation points detected for $\beta = 15$ (Figures 3 and 5). The result, shown in Figure 7, is in agreement with [7].

4.2. Colpitts oscillator

The second example of dynamical system considered is a Colpitts oscillator, which cannot be easily analysed with the semi-analytical approach in [7]. The circuit, shown in Figure 8, is modelled by

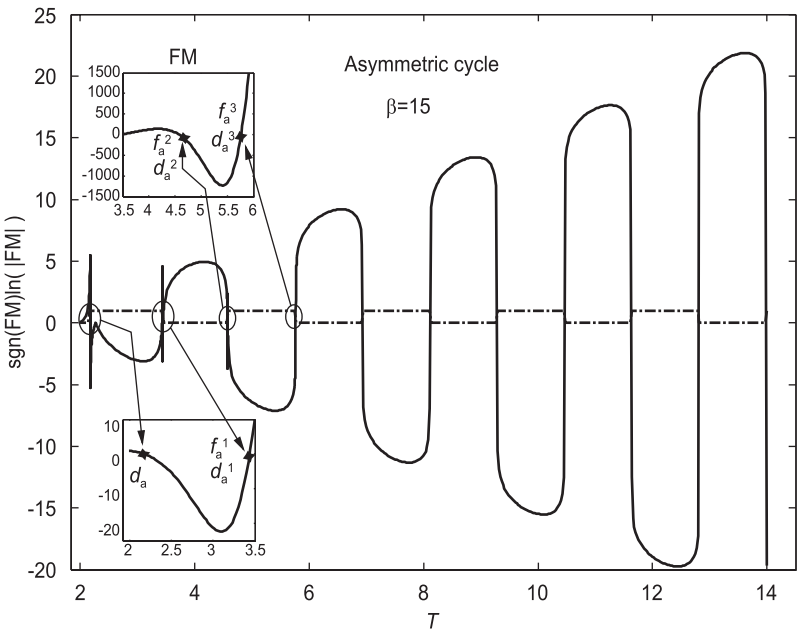

Figure 5. Chua's circuit: T dependence of the real part of the FM responsible of bifurcations for the asymmetric limit cycle. The dash-dotted line represents a function equal to 0 if the FE nearest to the real axis is real, and to 1 if it is complex.

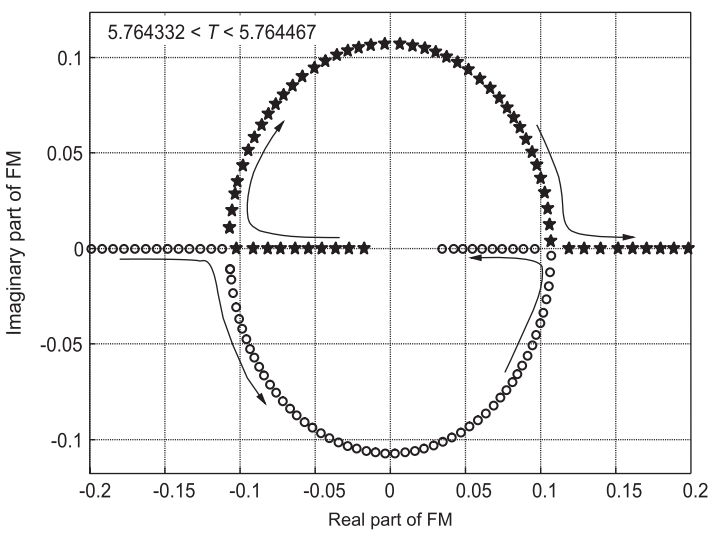

Figure 6. Chua's circuit: evolution in the complex plane of the FMs not identically equal to 1 for the asymmetric limit cycle between d_{a}^3 and f_{a}^3 as a function of the cycle period T.

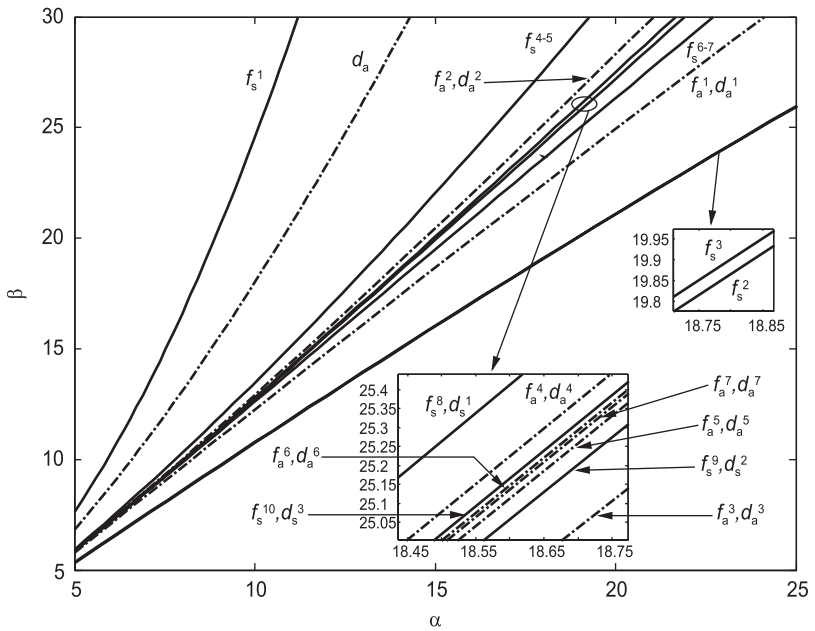

Figure 7. Bifurcation diagram in the parameter space (α, β) for several flip and fold bifurcations of both the symmetric and asymmetric Chua's circuit limit cycles.

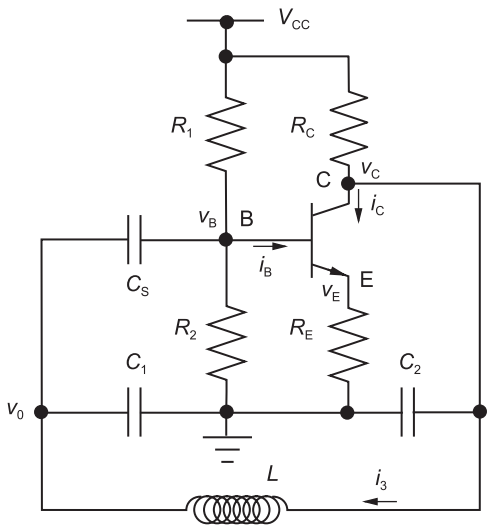

Figure 8. Circuit of the Colpitts oscillator.

assuming a static approximation for the bipolar transistor, which is described by the memoryless simplified model:

$$i_{\mathrm{B}} = I_{\mathrm{S}}\left[\exp\left(\frac{v_{\mathrm{BE}}}{V_{\mathrm{T}}}\right) - 1\right], \quad i_{\mathrm{E}} = \beta_{\mathrm{F}} i_{\mathrm{B}} \tag{34}$$

where I_{S} and β_{F} are constants, $V_{\mathrm{T}} = 26\,\mathrm{mV}$ at room temperature, and $v_{\mathrm{BE}} = v_{\mathrm{B}} - v_{\mathrm{E}}$. The circuit is described by the following MNA equations:

$$\begin{aligned}
C_2\frac{\mathrm{d}v_{\mathrm{C}}}{\mathrm{d}t} + i_3 + i_{\mathrm{C}} + \frac{v_{\mathrm{C}} - V_{\mathrm{CC}}}{R_{\mathrm{C}}} &= 0\\
L\frac{\mathrm{d}i_3}{\mathrm{d}t} - v_{\mathrm{C}} + v_0 &= 0\\
C_{\mathrm{S}}\frac{\mathrm{d}}{\mathrm{d}t}(v_{\mathrm{B}} - v_0) - C_1\frac{\mathrm{d}v_0}{\mathrm{d}t} + i_3 &= 0\\
C_{\mathrm{S}}\frac{\mathrm{d}}{\mathrm{d}t}(v_{\mathrm{B}} - v_0) + \frac{v_{\mathrm{B}}}{R_2} + \frac{v_{\mathrm{B}} - V_{\mathrm{CC}}}{R_1} + i_{\mathrm{B}} &= 0\\
\frac{v_{\mathrm{E}}}{R_{\mathrm{E}}} - i_{\mathrm{C}} - i_{\mathrm{B}} &= 0
\end{aligned} \tag{35}$$

which, completed by the constitutive relations (34), allow for the computation of the circuit working point. Substituting Equation (34) into Equation (35) and defining the normalized variables

$$x_1 = \frac{v_0}{V_{\mathrm{T}}}, \quad x_2 = \frac{R_{\mathrm{C}} i_3}{V_{\mathrm{CC}}}, \quad x_3 = \frac{v_{\mathrm{C}}}{V_{\mathrm{T}}} \tag{36}$$

$$x_4 = \frac{v_{\mathrm{B}}}{V_{\mathrm{T}}}, \quad x_5 = \frac{v_{\mathrm{E}}}{V_{\mathrm{T}}}, \quad \tau = \omega_0 t \tag{37}$$

the system equations are written as

$$\begin{aligned}
x_2 + \left(\nu + \alpha_2\frac{\mathrm{d}}{\mathrm{d}\tau}\right)x_3 + \beta_{\mathrm{F}}\xi[\exp(x_4 - x_5) - 1] - 1 &= 0\\
x_1 + \lambda\frac{\mathrm{d}x_2}{\mathrm{d}\tau} - x_3 &= 0\\
(\alpha + \alpha_1)\frac{\mathrm{d}x_1}{\mathrm{d}\tau} - x_2 - \alpha\frac{\mathrm{d}x_4}{\mathrm{d}\tau} &= 0\\
\alpha\frac{\mathrm{d}x_1}{\mathrm{d}\tau} + \left(\nu\gamma\rho + \alpha\frac{\mathrm{d}}{\mathrm{d}\tau}\right)x_4 + \xi[\exp(x_4 - x_5) - 1] - \rho &= 0\\
\nu\rho_1 x_5 - (\beta_{\mathrm{F}} + 1)\xi[\exp(x_4 - x_5) - 1] &= 0
\end{aligned} \tag{38}$$

where the normalization frequency is $\omega_0 = \sqrt{C_1 + C_2}/\sqrt{LC_1C_2}$, and the following parameters are defined:

$$\alpha = \omega_0 C_S R_C \frac{V_T}{V_{CC}}, \quad \alpha_1 = \alpha \frac{C_1}{C_S}, \quad \alpha_2 = \alpha \frac{C_2}{C_S} \tag{39}$$

$$v = \frac{V_T}{V_{CC}}, \quad \rho = \frac{R_C}{R_1}, \quad \rho_1 = \frac{R_C}{R_E} \tag{40}$$

$$\gamma = \frac{R_1 + R_2}{R_2}, \quad \lambda = \omega_0 \frac{L V_{CC}}{R_C V_T}, \quad \xi = \frac{R_C I_S}{V_{CC}} \tag{41}$$

System (38) is of the form (1), where $\mathbf{q}(\mathbf{x}) = \mathbf{C}\mathbf{x}$ is a linear relation characterized by the noninvertible matrix $\mathbf{C}$

$$\mathbf{C} = \begin{bmatrix} 0 & 0 & v + \alpha_2 & 0 & 0 \\ 0 & \lambda & 0 & 0 & 0 \\ \alpha + \alpha_1 & 0 & 0 & -\alpha & 0 \\ \alpha & 0 & 0 & \alpha & 0 \\ 0 & 0 & 0 & 0 & 0 \end{bmatrix} \tag{42}$$

and the nonlinear function $\mathbf{g}(\mathbf{x})$ is

$$\mathbf{g}(\mathbf{x}) = \begin{bmatrix} x_2 + v x_3 + \beta_F \xi [\exp(x_4 - x_5) - 1] - 1 \\ x_1 - x_3 \\ -x_2 \\ v\gamma\rho x_4 + \xi[\exp(x_4 - x_5) - 1] - \rho \\ v\rho_1 x_5 - (\beta_F + 1)\xi[\exp(x_4 - x_5) - 1] \end{bmatrix} \tag{43}$$

Therefore, $M = 5$ and $m = 4$. Notice also that, since $\mathbf{C}(\tau)$ is independent of τ, $\dot{\mathbf{C}} = \mathbf{0}$ and $\hat{\mathbf{A}}' = \hat{\mathbf{A}}$.

The circuit has been simulated with the HB method with $N_H = 15$, and assuming for the parameters the values

$$R_2 = 100\,\text{k}\Omega, \quad R_C = 4.9\,\text{k}\Omega, \quad R_E = 90\,\Omega \tag{44}$$

$$C_1 = 0.3\,\mu\text{F}, \quad C_2 = 9.09\,\text{nF}, \quad C_S = 1\,\mu\text{F} \tag{45}$$

$$V_{CC} = 15\,\text{V}, \quad L = 27.78\,\text{nH} \tag{46}$$

while the transistor parameters are $\beta_F = 100$ and $I_S = 10^{-18}$ A.

Of the $m = 4$ FMs not identically equal to 0, one is equal to 1 (as expected for an oscillator), two are complex conjugate with negative real part, and the fourth is real, positive and close to 1. We have determined the oscillator limit cycle as a function of two parameters (R_1 and α_1, see

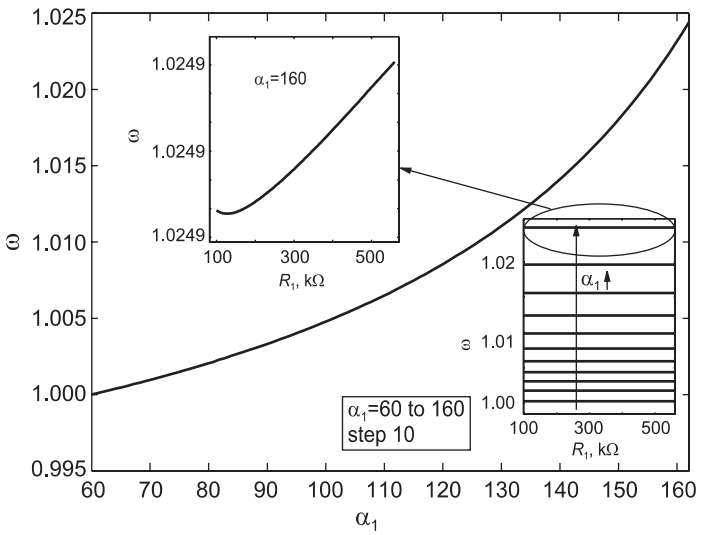

Figure 9. Colpitts oscillator: angular frequency of the limit cycle as a function of α_1 and R_1 parameters. The main curve is plotted for $R_1 = 100\,\mathrm{k}\Omega$

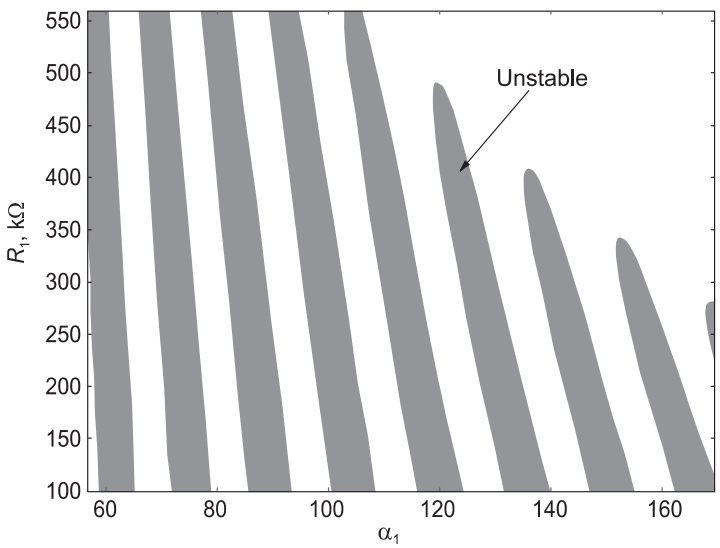

Figure 10. Colpitts oscillator: regions of unstable operation in the (α_1, R_1) parameter plane. The frontiers of the shaded regions represent fold bifurcation curves, since the FM is real and positive.

Figure 9), and computed the corresponding FMs. In several regions of this parameter space the cycle becomes unstable, i.e. one FM exhibits magnitude larger than 1, as shown in Figure 10. A similar result was obtained in [17], making use of the describing function technique. Notice that the borders of the unstable regions represent fold bifurcation curves, since the represented FM is

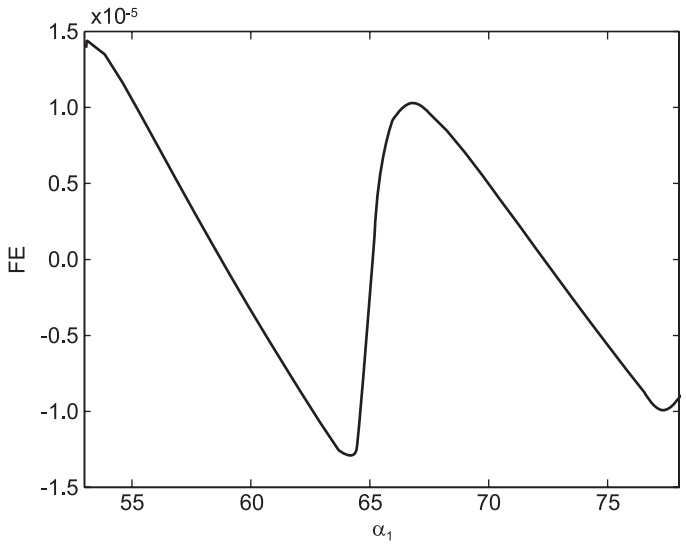

Figure 11. Colpitts oscillator: evolution in the complex plane of the FE as a function of parameter α_1.

real and positive. The evolution in the complex plane of the corresponding FE as a function of α_1 (for R_1 held constant to 100 kΩ) is represented in Figure 11, where the limit cycle is shown to undergo a period-doubling bifurcation for $\alpha_1 < 60$ (see also Figure 10).

5. CONCLUSION

We have proposed a general numerical technique for the assessment of the stability properties of periodic solutions in nonlinear dynamical systems described by differential-algebraic equations (DAEs), based on the estimation of the Floquet exponents (FEs) of the steady-state solution performed directly in the frequency domain. This allows to directly extend the standard harmonic balance (HB) technique, widely used for the determination of the steady state, to the perturbative stability analysis, since the matrices involved in the FE calculation are strictly related to the Jacobian matrices exploited for the Newton iterative solution of the HB problem. Moreover, the approach can in principle be directly implemented even in commercial CAD tools for circuit analysis, since the DAE form is typically found in the MNA equations such simulators usually employ.

In order to validate the approach, we have determined the stability and bifurcations of the limit cycles of the well-known Chua's circuit with cubic nonlinearity, and of a standard Colpitts oscillator. A parametric analysis has been carried out, allowing for the accurate determination of a wide variety of bifurcation curves, both for the cases of fold and flip bifurcations.

REFERENCES

1. Suárez A, Quéré R. *Stability Analysis of Nonlinear Microwave Circuits*. Artech House: Norwood, 2003.
2. Farkas M. *Periodic Motions*. Springer: New York, 1994.
3. Demir A. Fully nonlinear oscillator noise analysis: an oscillator with no asymptotic phase. *International Journal of Circuit Theory and Applications* 2007; **35**:175–203.

4. Kundert KS, Sangiovanni-Vincentelli A, White JK. *Steady-state Methods for Simulating Analog and Microwave Circuits*. Kluwer Academic Publishers: Boston, 1990.
5. Kuznetov YA. *Elements of Applied Bifurcation Theory*. Springer: New York, 1995.
6. Basso M, Genesio R, Tesi A. A frequency method for predicting limit cycle bifurcations. *Nonlinear Dynamics* 1997; **13**:339–360.
7. Bonani F, Gilli M. Analysis of stability and bifurcations of limit cycles in Chua's circuit through the harmonic balance approach. *IEEE Transactions on Circuits and Systems I*: *Fundamental Theory and Applications* 1999; **46**(8):881–890.
8. Mees AI. *Dynamics of Feedback Systems*. Wiley: Chichester, 1981.
9. Chua LO, Desoer CA, Kuh ES. *Linear and Nonlinear Circuits*. McGraw-Hill: New York, 1987.
10. Lamour R, März R, Winkler R. How Floquet theory applies to index-1 differential algebraic equations. *Journal of Mathematical Analysis and Applications* 1998; **217**:372–394.
11. Demir A. Floquet theory and non-linear perturbation analysis for oscillators with differential-algebraic equations. *International Journal of Circuit Theory and Applications* 2000; **28**:163–185.
12. Bai Z, Demmel J, Dongarra J, Ruhe A, van der Vorst H. *Templates for the Solution of Algebraic Eigenvalue Problems*: *A Practical Guide*. SIAM: Philadelphia, PA, 2000.
13. Press WH, Teukolsky SA, Vetterling WT, Flannery BP. *Numerical Recipes in Fortran 77* (2nd edn). Cambridge University Press: Cambridge, 1997.
14. Duan X, Mayaram K. Frequency-domain simulation of ring oscillators with a multiple-probe method. *IEEE Transactions on Computer-aided Design of Integrated Circuits and Systems* 2006; **25**:2833–2842.
15. Duan X, Mayaram K. Robust simulation of high-Q oscillators using a homotopy-based harmonic balance method. *IEEE Transactions on Computer-aided Design of Integrated Circuits and Systems* 2006; **25**:2843–2851.
16. Khibnik AI, Roose D, Chua LO. On periodic orbits and homoclinic bifurcations in Chua's circuit with a smooth nonlinearity. *International Journal of Bifurcation and Chaos* 1993; **3**:363–384.
17. Maggio GM, Kennedy MP, Gilli M. An approximate analytical approach for predicting period-doubling in the Colpitts oscillator. *Proceedings of IEEE International Symposium on Circuits and Systems*, vol.3, Monterey, CA, U.S.A., 1998; 671–674.